

The Supernova Remnant W44: confirmations and challenges for cosmic-ray acceleration

M. Cardillo^{1,2}, M. Tavani^{1,2,3}, A. Giuliani^{3,4}, S. Yoshiike⁵, H. Sano⁵, T. Fukuda⁵, Y. Fukui⁵, G. Castelletti⁶, and G. Dubner⁶

¹ INAF/IAPS, I-00133 Roma, Italy
e-mail: mcardillo@roma2.infn.it

² Dip. di Fisica, Univ. Tor Vergata, I-00133 Roma, Italy

³ CIFS-Torino, I-10133 Torino, Italy

⁴ INAF/IASF-Milano, I-20133 Milano, Italy

⁵ Department of Physics and Astrophysics, Nagoya University, Furo-cho, Chikusa-ku, Nagoya, Aichi 464-8601, Japan

⁶ Instituto de Astronomía y Física del Espacio (IAFE), CC.67, Suc.28, 1428, Buenos Aires, Argentina

Received / Accepted

ABSTRACT

The middle-aged supernova remnant (SNR) W44 has recently attracted attention because of its relevance regarding the origin of Galactic cosmic-rays. The gamma-ray missions AGILE and Fermi have established, for the first time for a SNR, the spectral continuum below 200 MeV which can be attributed to neutral pion emission. Confirming the hadronic origin of the gamma-ray emission near 100 MeV is then of the greatest importance. Our paper is focused on a global re-assessment of all available data and models of particle acceleration in W44, with the goal of determining on a firm ground the hadronic and leptonic contributions to the overall spectrum. We also present new gamma-ray and CO NANTEN2 data on W44, and compare them with recently published AGILE and Fermi data. Our analysis strengthens previous studies and observations of the W44 complex environment and provides new information for a more detailed modeling. In particular, we determine that the average gas density of the regions emitting 100 MeV- 10 GeV gamma-rays is relatively high ($n \sim 250 - 300 \text{ cm}^{-3}$). The hadronic interpretation of the gamma-ray spectrum of W44 is viable, and supported by strong evidence. It implies a relatively large value for the average magnetic field ($B \geq 10^2 \mu\text{G}$) in the SNR surroundings, sign of field amplification by shock-driven turbulence. Our new analysis establishes that the spectral index of the proton energy distribution function is $p_1 = 2.2 \pm 0.1$ at low energies and $p_2 = 3.2 \pm 0.1$ at high energies. We critically discuss hadronic versus leptonic-only models of emission taking into account simultaneously radio and gamma-ray data. We find that the leptonic models are disfavored by the combination of radio and gamma-ray data. Having determined the hadronic nature of the gamma-ray emission on firm ground, a number of theoretical challenges remains to be addressed.

Key words. acceleration of particles, astroparticle physics, shock waves, radiation mechanisms, Supernova Remnants, gamma-rays

1. Introduction

Cosmic-rays (CRs) are highly energetic particles (with kinetic energies up to $E = 10^{20}$ eV) mainly composed by protons and nuclei with a small percentage of electrons (1%). Currently, the CR origin is one of the most important problems of high-energy astrophysics, and the issue is the subject of very intense research (Fermi 1949; Ginzburg & Syrovatskii 1964; Berezhinskii et al. 1990). For recent reviews see Helder et al. (2012) and Aharonian (2012). Focusing on CRs produced in our Galaxy (energies up to the so called “knee”, $E = 10^{15}$ eV), strong shocks in Supernova Remnants (SNRs) are considered the most probable CR sources (e.g., Ginzburg & Syrovatskii 1964). This hypothesis is supported by several “indirect” signatures indicating the presence of ultra-high energy electrons (recent review in Vink 2012). However, the final proof for the origin of CRs up to the knee can only be obtained through two fundamental signatures. The first one is the identification of sources emitting a photon spectrum up to PeV energies. The second one is the detection of a clear gamma-ray signature of π^0 decay in Galactic sources. Both indications are quite difficult to obtain. The “Pevatron” sources are notoriously hard to find (see Aharonian 2012, for a review), and the neutral pion decay signature is not easy to identify because

of the possible contribution from co-spatial leptonic emission. Hadronic (expected to produce the π^0 decay spectral signature) and leptonic components can in principle be distinguished in the 50-200 MeV energy band, where they are expected to show different behaviors.

Over the last five years AGILE and Fermi, together with ground telescopes operating in the TeV energy range (HESS, VERITAS and MAGIC), collected a great amount of data from SNRs (Abdo et al. 2009, 2010a,b,c,e,d, 2011; Acciari et al. 2009; Tavani et al. 2010; Acciari et al. 2010, 2011; Aharonian et al. 2001, 2007, 2008; Aleksic, J. et al. 2012; Giordano et al. 2012; Giuliani et al. 2010; Hewitt et al. 2012; Katsuta et al. 2012; Lemoine et al. 2012) providing important information and challenging theoretical models. For example, most of the observed SNRs appear to have a spectrum steeper than the one expected from linear and non-linear diffusive shock acceleration models (DSA) of index near 2 (and possibly convex spectrum Bell 1987; Malkov & Drury 2001; Blasi et al. 2005). W44 is one of the most interesting SNRs observed so far; it is a middle-aged SNR, bright at gamma-ray energies and quite close to us. Its gamma-ray spectral index (indicative of the underlying proton/ion distribution in the hadronic model) is $p \sim 3$, in apparent contradiction with DSA

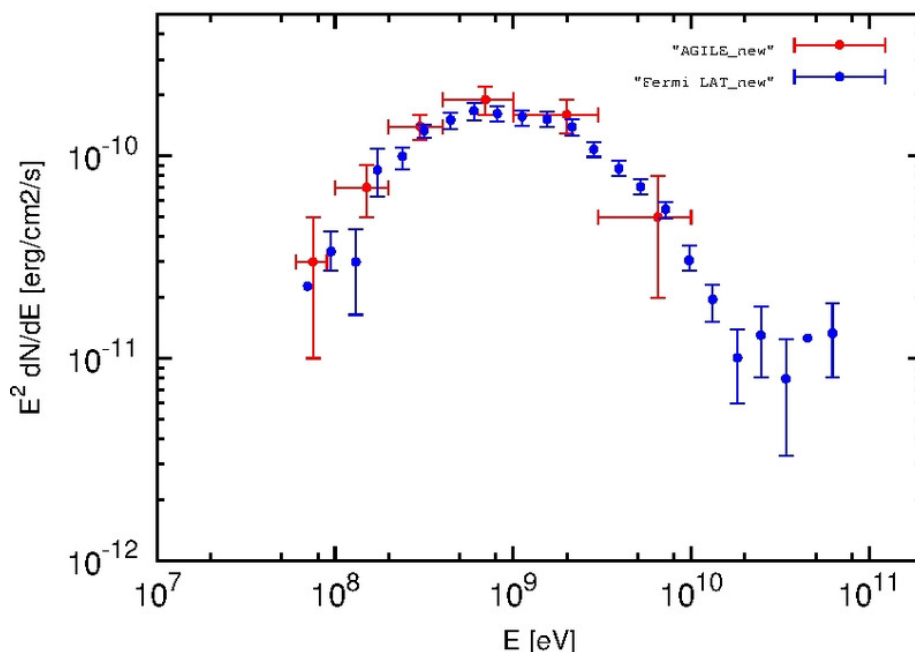


Fig. 1. AGILE new gamma-ray spectrum of SNR W44 (red data points) superimposed with the Fermi-LAT data from Ackermann et al. (2013) (blue data points).

models. W44 is therefore an ideal system to study CR acceleration in detail. The AGILE data analysis of this remnant provided for the first time information below $E = 200$ MeV, showing the low-energy steepening in agreement with the hadronic interpretation (Giuliani et al. 2011). Recently, an analysis of Fermi-LAT data confirms these results (Ackermann et al. 2013).

In this paper, we present a new analysis of AGILE data together with a re-assessment of CO and radio data on W44. We also compare our results with those obtained from Fermi-LAT data. In section 2, we summarize the most relevant facts about W44, and in section 3, we present an updated view on the AGILE gamma-ray data and on the CO and radio data of this SNR. In section 4, we discuss hadronic and leptonic models in the light of our refined analysis. The implications of this work are discussed in section 5. We provide relevant details about our modeling in the Appendices.

2. The supernova remnant W44

W44 is a middle-aged ($\sim 20,000$ yrs old) SNR located in the Galactic Plane ($l, b = (34.7, -0.4)$), at a distance $d \sim 3.1$ kpc (Clark & Caswell 1976; Wolszczan et al. 1991, Fang et al. (2013) report 1.9 kpc.). Multiwavelength observations revealed interesting features. In the radio band, W44 shows a quasi-elliptical shell (Castelletti et al. 2007, and references therein); the radio shell asymmetry is probably due to expansion in an inhomogeneous ISM. In the North-West side of the remnant, in correlation with a peak of the radio emission, there is bright [SII] emission characteristic of shock-excited radiative filaments (Giacani et al 1997). In the South-East side, instead, there is a molecular cloud (MC) complex embedded in the SNR shell and interacting with the source (Wootten et al. 1977; Rho et al. 1994). OH masers (1720 MHz) found in correspondence with the SNR/MC region, confirm their interaction (Claussen et al. 1997; Hoffman et al. 2005). Wolszczan et al. (1991) reported the discovery of the radio pulsar PSR B1853+01, located in the South part of the remnant and surrounded by a cometary-shaped pulsar wind nebula (PWN) (Frail et al. 1996). This system, however, does not appear to be correlated with the detected gamma-ray emission. X-ray observations of W44 by the Einstein Observatory (Watson et al. 1983) showed centrally peaked emission, later confirmed by Chandra data (Shelton et al. 2004).

The first report on W44 in the gamma-ray band was by Fermi-LAT (Abdo et al. 2010e) that showed a GeV emission morphology in apparent good correlation with the radio shell. The Fermi-LAT energy power spectrum of W44 showed a prominent peak near 1 GeV and a clear decrease at higher energies with a quite steep spectrum of photon index near 3 (Abdo et al. 2010e). Early processing of Fermi-LAT data had a low-energy threshold of 200 MeV, thus limiting its ability to identify a neutral pion signature. It is then not surprising that in addition to hadronic models also leptonic models predicting bremsstrahlung emission below 200 MeV could not be excluded. The relatively large gamma-ray brightness of W44 and the good spectral capability of AGILE near 100 MeV (Tavani et al. 2008; Vercellone et al. 2008, 2009) stimulated a thorough investigation of this supernova remnant with the AGILE data. The AGILE gamma-ray spectrum in the range 50 MeV - 10 GeV confirms the high-energy steep slope up to 10 GeV, and, remarkably, identifies for the first time a spectral decrease below 200 MeV as expected from neutral pion decay (Giuliani et al. 2011, hereafter G11). In the analysis of G11, both leptonic and hadronic models were considered to fit both AGILE and Fermi-LAT data. Proper consideration was given to the constraints derived from VLA radio data and NANTEN CO data for the ambient magnetic field and density, respectively. In G11, the best model was determined to be dominated by hadronic emission with a proton distribution of spectral index $p_2 = 3.0 \pm 0.1$ and a low-energy cut-off at $E_c = 6 \pm 1$ GeV. The W44 gamma-ray morphology determined by AGILE agrees well with the emission detected by Fermi-LAT below 1 GeV. Furthermore, a correlation of gamma-ray emission with CO emission is observed, indicating that most of the gamma-ray emission can be associated with the SNR/MC interaction. A possible large-scale influence of escaping particles accelerated at the W44 SNR shock

was studied by Uchiyama et al. (2012) who noticed the existence of far and bright gamma-ray bright MCs. A new important contribution was recently produced by the Fermi-LAT team that revisited the gamma-ray emission from W44 (Ackermann et al. 2013, hereafter A13). This work was motivated also by the improvement in the LAT data analysis that permits a better study of the spectrum near 100 MeV (Ackermann et al. 2012). The new gamma-ray spectrum of W44 by Fermi-LAT fully confirms the AGILE spectrum below 200 MeV (Ackermann et al. 2013, for a comparison of AGILE and new Fermi-LAT data, see Fig. 6 in Appendix A). The analysis in A13 tends to exclude a leptonic-only contribution to the gamma-ray emission because it requires a very large density ($n \sim 650 \text{ cm}^{-3}$). Their best hadronic model, with an *assumed* surrounding medium density $n \sim 100 \text{ cm}^{-3}$, is based on a smoothed broken power-law hadronic distribution with a break energy $E_{br} = 22 \text{ GeV}$ and indexes $p_1 = 2.36$ for $E < E_{br}$, and $p_2 = 3.5$ for $E > E_{br}$. Model parameters in A13 differ from those considered earlier in Abdo et al. (2010e). Apparently, in the hadronic modeling of A13 bremsstrahlung emission is not considered to be relevant, even though in principle this process could provide a non-negligible contribution to the gamma-ray emissivity. An important feature of the SNR W44 spectrum is its slope at GeV energies: the index $p \sim 3$ is substantially steeper than the range plausibly expected in linear and non-linear DSA models. In Malkov et al. (2011) this spectral feature is explained by Alfvén damping in the presence of a relatively large-density medium where acceleration occurs. The W44 environment is quite challenging in its morphology, and requires a reanalysis of its properties in the context of the crucial implications for the acceleration mechanism of CRs. We present here a new analysis of AGILE data together with a revised assessment of the W44 surrounding environment based on new CO data obtained from the NANTEN2 telescope.

3. New AGILE data analysis

We performed a global reassessment of the AGILE data on W44, including new gamma-ray data obtained until June, 2012. The new data were obtained using the updated AGILE data archive, available at the ASDC site (www.asdc.asi.it). The analysis procedure is the same described in G11¹ except for the map bin-size (that is now wider than before for an analysis focused on extended features) and the substantially more extended observing period.

3.1. Morphology

The upper left panel of Fig. 2 shows the W44 AGILE gamma-ray map in the 400-10000 MeV energy range² with radio contours from VLA (green contour levels). The upper right panel shows the NANTEN2 telescope CO map in two velocity channels, 41 and 43 km/s, with AGILE (magenta) and VLA (white) contours. Gamma-ray emission appears to be mostly concentrated near a high-density region, (bottom panel of the Fig. 2), indicating that most of the W44 gamma-ray emission is coincident with a site of SNR/MC interaction. This MC could be at some distance from the remnant or embedded in it. The CO maps (Fig. 2, medium

panel) show the presence of a large molecular cloud complex with four different peaks at (34.8,-0.8), (34.75,-0.5), (35.1,-0.2), and (34.65,-0.1), respectively, indicated by the thick white lines. Each of these peaks reaches densities of about 10^3 cm^{-3} , for an estimated average density in the SNR shell of $n_{av} \sim 200 \text{ cm}^{-3}$ (Yoshiike et al. 2013). A good correlation with the gamma-ray emission is in correspondence with the peak at (34.7,-0.5).

3.2. Spectrum

Fig. 1 shows the AGILE gamma-ray spectrum together with the recently updated Fermi-LAT data from Ackermann et al. (2013). The AGILE spectrum is composed by six energy bins between 50 MeV and 10 GeV and our error-bars takes into account statistical errors³. The measured flux of the source above 400 MeV is $F = (23 \pm 2) \times 10^{-8} \text{ ph cm}^{-2} \text{ s}^{-1}$. We notice the good agreement between the two spectra. Especially important is the confirmation of the drastic spectral decrement below 200 MeV, a crucial feature that will be discussed below. Both AGILE and Fermi-LAT spectra differ somewhat from the previously published spectra in G11 and Abdo et al. (2010e) (see Appendix A).

4. Modeling

We model the radio, AGILE and Fermi-LAT spectral data by hadronic and leptonic-only scenarios, taking into account the new NANTEN2 CO data providing a value for the ISM density in the SNR surroundings⁴, $n_{av} \approx 250 \text{ cm}^{-3}$ (Yoshiike et al. 2013). This value of the average gaseous density surrounding the gamma-ray emission is substantially larger than the one assumed in G11 and A13 ($n = 100 \text{ cm}^{-3}$). Since the AGILE gamma-ray emission is strongly correlated with one of the CO peaks, in the following we consider an average density $n \approx 300 \pm 50 \text{ cm}^{-3} > n_{av}$. In modeling the spectra, we consider the most statistically significant Fermi-LAT data up to 50 GeV.

4.1. Hadronic Models

We assume that the gamma-ray emission spectrum is due to the combined contribution of hadronic π^0 emission and leptonic bremsstrahlung emission, considering the proton component as the main one. For hadronic emission, we use the formalism explained in Kelner et al. (2006) that is a good approximation of the exact solution. We consider a proton distribution in total energy E , rather than in kinetic energy $E_k = E - m_p c^2$, following Simpson (1983) and Dermer (1986) but with δ -function approximation for the cross section (Aharonian 2004). This approximation provides that a fixed fraction of proton energy is converted to π^0 energy. Even if the distribution is broad, this method gives results with good accuracy as long as the proton spectrum is smooth and broad (e.g., power-law). We fit the gamma-ray data assuming different types of proton distributions (see Fig. 3):

- a simple power-law with a high-energy cut-off (**model H1**):

$$\frac{dN_{p,1}}{dE} = K_p \left(\frac{E}{E_c^p} \right)^{-p_1} e^{-\frac{E}{E_c^p}} \quad (1)$$

¹ For more details about the background model, software and likelihood technique, see Giuliani et al. (2004, 2006); Bulgarelli et al. (2012); Chen et al. (2013).

² The different morphology of the gamma-ray emission compared to that presented in G11 is influenced by binning. In G11 we used $0.02^\circ \times 0.02^\circ$ bins, instead here we make the choice of a $0.05^\circ \times 0.05^\circ$ binning.

³ The systematic errors in the canonical energy band (100 MeV-3 GeV) are of order of 20% – 30% of the statistical errors (Chen et al. 2013).

⁴ Yoshiike et al. (2013) use a H2/CO ratio equals to $X_{CO} = 1.56 \times 10^{20} \text{ cm}^{-2}/\text{K/km/s}^{-1}$ (see also Hunter et al., (1997)) that we use as a reference value. This value of X_{CO} is known to be uncertain within a factor of at least 2 (see, e.g., Strong et al. (2004)).

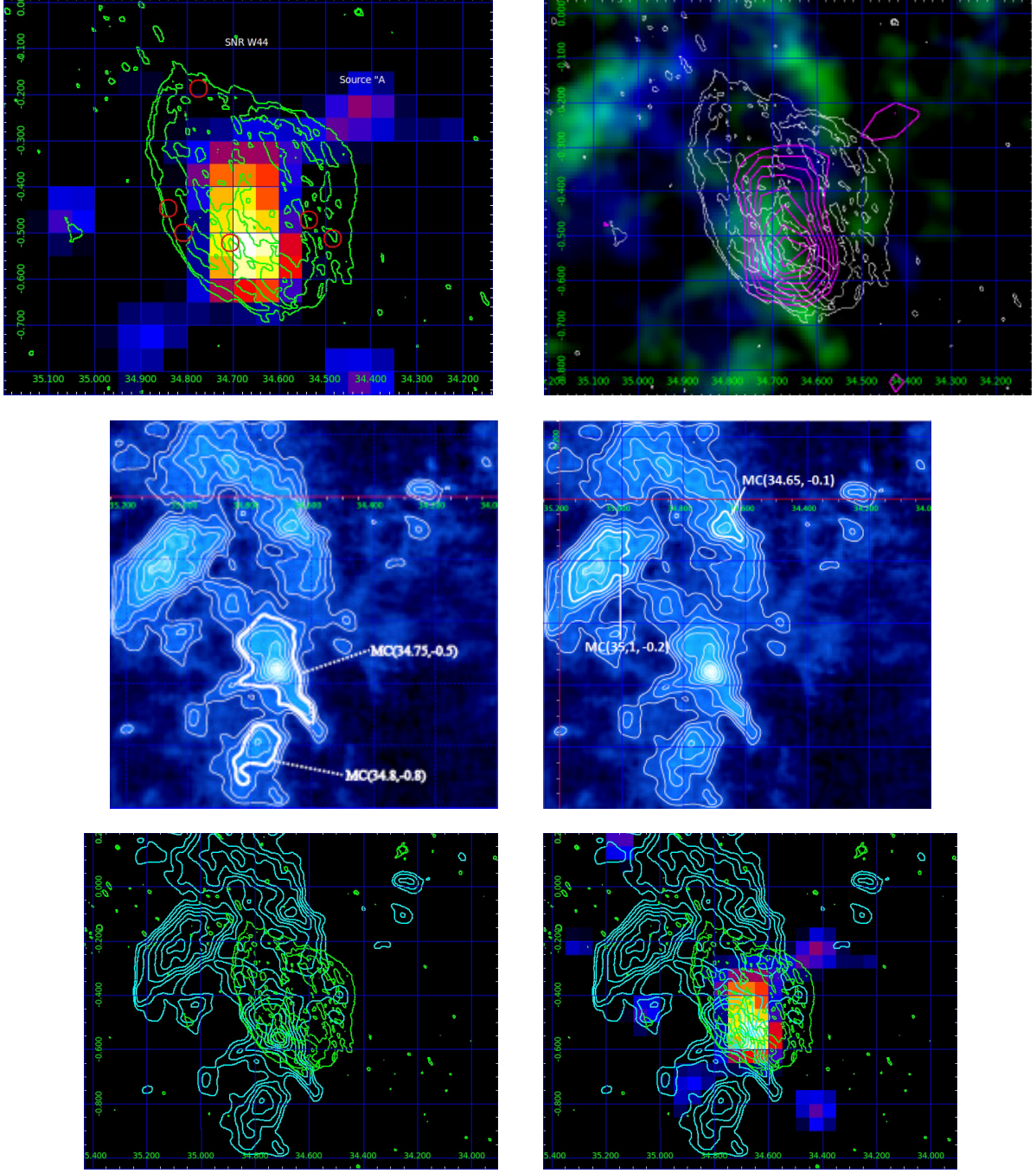


Fig. 2. (Upper Left Panel): AGILE gamma-ray intensity map (in Galactic coordinates) of the W44 region in the energy range 400 MeV-10 GeV, obtained integrating all available data collected during the period May 2007 and June 2012. Pixel size is $0.05^\circ \times 0.05^\circ$ with a 3-bin Gaussian smoothing. Green contours show the 324 MHz radio continuum flux density detected by the Very Large Array (Castelletti et al. 2007) and red circles indicate detected OH masers (Claussen et al. 1997). (Upper Right Panel): combined CO data from the NANTEN2 observatory superimposed with the AGILE gamma-ray data contours (magenta) above 400 MeV of the W44 region (map in Galactic coordinates) and VLA contours (white). CO data have been selected in the velocity range 40-43 km s⁻¹, corresponding to a kinematic distance compatible with the W44 distance. (Medium Left and Right Panels): NANTEN2 CO integrated maps with CO contours (40-43 km/s). Thick white lines show the four CO peaks. (Bottom Left Panel): NANTEN2 CO integrated contours (40-43 km/s, cyan) and VLA contours (green). (Bottom Right Panel): AGILE intensity map (400 MeV-10 GeV) with NANTEN2 (cyan) and VLA (green) contours.

– a smoothed broken power-law (**model H2**):

$$\frac{dN_{p,2}}{dE} = K_p \left(\frac{E}{E_{br}^p} \right)^{-p_1} \left(\frac{1}{2} \left(1 + \frac{E}{E_{br}^p} \right) \right)^{p_1-p_2} \quad (2)$$

– a broken power-law (**model H3**):

$$\frac{dN_{p,3}}{dE} = \begin{cases} K_{p,1} \left(\frac{E}{E_{br}^p} \right)^{-p_1} & \text{if } E < E_{br} \\ K_{p,2} \left(\frac{E}{E_{br}^p} \right)^{-p_2} & \text{if } E > E_{br} \end{cases} \quad (3)$$

Table 1. Hadronic model parameters: p_1 is the proton spectral index before the break, p_2 is the proton spectral index above the break, E_{br}^p is the proton break energy, E_c^p is the proton cut-off energy, K_p and K_e are proton and electron normalization constants, and $\frac{\chi^2}{n-1}$ is the reduced chi-square.

Models	p_1	p_2	E_{br}^p [GeV]	E_c^p [GeV]	K_p [1/MeV/cm ³]	K_e [1/MeV/cm ³]	$\chi^2/n-1$
H1	2.0 ± 0.1	-	-	45 ± 1	2×10^{-14}	4×10^{-14}	2
H2	1.7 ± 0.1	3.5 ± 0.1	16 ± 1	-	3.9×10^{-14}	7×10^{-14}	1.8
H3	2.2 ± 0.1	3.2 ± 0.1	20 ± 1	-	$K_1 \sim 1.8 \times 10^{-13}, K_2 \sim 1.5 \times 10^{-13}$	1.5×10^{-12}	1.5

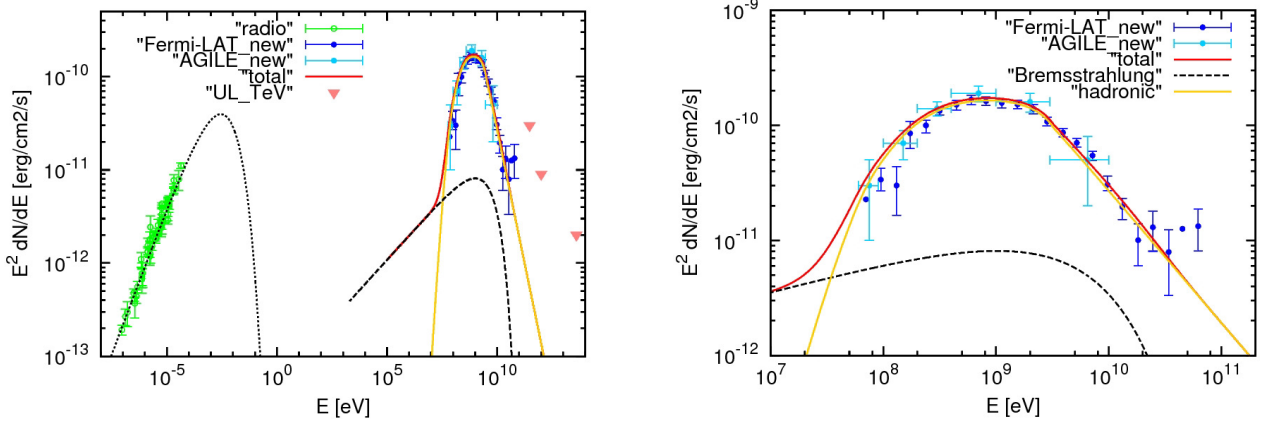


Fig. 4. Our best hadronic model, H3, of the broad-band spectrum of the SNR W44 superimposed with radio (data points in green color) and gamma-ray data of Fig. 1 (in blue and cyan color). Proton distribution in Eq. 3 with index $p_1 = 2.2 \pm 0.1$ (for $E < E_{br}$), $p_2 = 3.2 \pm 0.1$ (for $E > E_{br}$) where $E_{br}^p = 20$ GeV. This model is characterized by $B = 210 \mu\text{G}$ and $n = 300 \text{ cm}^{-3}$. The yellow curve shows the neutral pion emission from the accelerated proton distribution discussed in the text. The black curves show the electron contribution by synchrotron (dot) and bremsstrahlung (dashed) emissions; the IC contribution is negligible. The red curve shows the total gamma-ray emission from pion-decay and bremsstrahlung. **(Left Panel):** SED from radio to gamma-ray band. **(Right Panel):** only gamma-ray part of the spectrum.

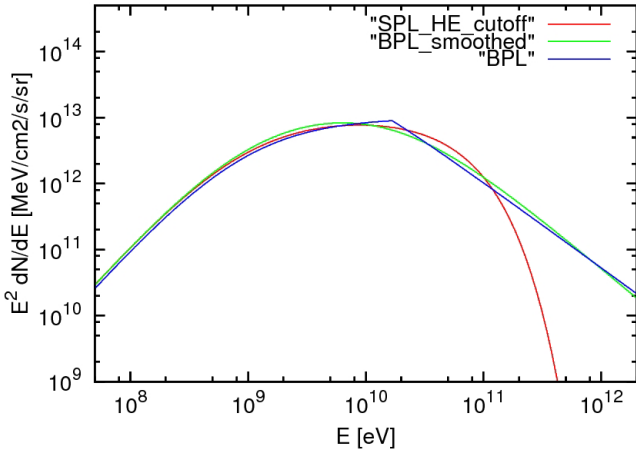


Fig. 3. Particle total energy distributions for our best hadronic models plotted vs the kinetic energy: a simple power-law with a high-energy cut-off at $E_c = 45$ GeV (Eq. 1, red), a smoothed broken power-law with $E_{br} = 16$ GeV (Eq. 2, green) and broken power-law with $E_{br} = 20$ GeV (Eq. 3, blue).

For leptons, in all hadronic models we used a simple power-law with a high energy cut-off:

$$\frac{dN_e}{dE} = K_e \left(\frac{E}{E_c^e} \right)^{-p'} e^{-\frac{E}{E_c^e}} \quad (4)$$

We fix only the parameters for which we have solid observational evidence; the average medium density, $n = 300 \text{ cm}^{-3}$ and the radio spectral index, $p' = 1.74$. We vary all other parameters such as the normalization constants, K_p and K_e , and the cut-off and break energies, E_c and E_{br} . Our results are summarized in Table 1 where we show the best models obtained according to the standard chi-square minimization test (Taylor 2000). Every model is discussed individually in Appendix 6. Here we present the properties of our best hadronic model H3. This is characterized by the distribution in Eq. 3 with $p_1 = 2.2 \pm 0.1$ (for $E < E_{br}$), $p_2 = 3.2 \pm 0.1$ (for $E > E_{br}$), and an energy break $E_{br}^p = 20$ GeV. The leptonic contribution to this model is given by a simple power-law for the electrons, with $p' = 1.74$, and $E_c^e = 12$ GeV (see Fig. 4). This model provides a proton energy $W^p = 5 \times 10^{49}$ erg and requires an average magnetic field in the emission region, $B = 210 \mu\text{G}$.

In our calculations we do not consider the so called "nuclear enhancement factor" (Dermer 2012) that takes into account helium contribution to the gamma-ray spectrum and this is of the order of 2. However, the only change due to this factor is a reduced proton energy density; our most important results and conclusions about spectral indices and parameter estimation are not affected in any way.

4.2. Leptonic-only Models

It is important to test the viability of leptonic-only models of gamma-ray emission from W44. We use the general expression for electron radiative processes as in Blumenthal & Gould (1970).

- Synchrotron emission - For a power-law electron distribution, it is convenient to use a δ -function approximation (e.g., Longair 2011) that can be expressed as:

$$\frac{dN}{dE_\gamma} = 4\pi \frac{1}{E_{ph}} \sigma_{th} U_B F_e(E_e) dE_e \left[\frac{1}{MeV s cm^{-3}} \right] \quad (5)$$

where $U_B = \frac{B^2}{8\pi} \text{ MeV cm}^{-3}$ is magnetic energy density, σ_{th} is Thompson cross section, $dE_e = \frac{m_e c^2}{2} \left(\frac{3}{4} \frac{1}{E_\gamma E_{ph}} \right)$ and $E_{ph} = \frac{Be}{2\pi m_e c}$ is the initial photon energy. For a power-law electron distribution proportional to $E^{-p'}$, the photon energy distribution is then proportional to $E^{-(\frac{p'+1}{2})}$.

- Bremsstrahlung emission - We used the general expression from Blumenthal & Gould (1970):

$$\frac{dN}{dE} = \alpha r_0^2 E^{-1} n \int dE_e F_e(E_e) E_e^{-2} \left[\left(2E_e^2 - 2E_e E + E^2 \right) \phi_1 - \frac{2}{3} E_e (E_e - E) \phi_2 \right] \left[\frac{1}{MeV s cm^{-3}} \right] \quad (6)$$

where n is the density, ϕ_1 and ϕ_2 are functions of electron energies, α is the fine structure constant and r_e is the electron classical radius. This can be used both in a totally ionized medium (weak shielding) and in the presence of neutrals (strong shielding); difference is only a logarithmic factor. For a power-law electron distribution proportional to E^{-p} , the photon energy distribution is then proportional to $E^{-p'}$.

- Inverse Compton emission

$$\frac{dN}{dE} = 4\pi \frac{1}{E_{ph}} \sigma_{kn} U_{ph} F_e(E_e) dE_e \left[\frac{1}{MeV s cm^{-3}} \right] \quad (7)$$

where U_{ph} energy density of the radiation field, σ_{kn} is Klein-Nishina cross section, $dE_e = \frac{m_e c^2}{2} \left(\frac{3}{4} \frac{1}{E_\gamma E_{ph}} \right)$ and E_{ph} is the interstellar radiation field initial photon energy.

In order to fit both gamma-ray and radio data, we consider a smoothed broken power-law leptonic distribution:

$$\frac{dN_{e,2}}{dE} = K_p \left(\frac{E}{E_{br}^e} \right)^{-p'_1} \left(\frac{1}{2} \left(1 + \frac{E}{E_{br}^e} \right) \right)^{p'_1 - p'_2} \quad (8)$$

Our assumption is that the same electron population produces both the gamma-ray and the radio fluxes through bremsstrahlung and synchrotron emissions, respectively. The spatial co-existence of radio filaments and sites of gamma-ray emission justifies this hypothesis. We fix the gaseous density value, $n = 300 \text{ cm}^{-3}$, from NANTEN2 data.

Our first leptonic-only model was developed (L1, see Table 2) fixing the electron spectral index at the value found from radio data analysis by Castelletti et al. (2007), $p'_1 = 1.74$ for $E < E_{peak}$. We found a high energy electron spectral index $p'_2 = 4.2 \pm 0.1$ above an energy break $E_{br}^e \sim 8 \text{ GeV}$ and a magnetic field $B \sim 25 \mu\text{G}$. However, fixing $p'_1 = 1.74$, we can fit radio synchrotron data but we cannot fit in any way the low-energy gamma-ray data (see

Fig. 5).

The second leptonic-only model was developed in order to fit gamma-ray data with the Bremsstrahlung emission (L2, see Table 2), changing the electron spectral index. We can fit low-energy gamma-ray data with an index $p'_1 = -2.5 \pm 0.1$ for $E < E_{br}^e$, very hard to explain. The other parameters found are $p'_2 = 3.4 \pm 0.1$ for $E > E_{br}^e$, $E_{br}^e \sim 500 \text{ MeV}$ and $B \sim 40 \mu\text{G}$.

5. Discussion

5.1. Models

Gamma-ray emission from SNRs can be produced in general by three different mechanisms: (1) relativistic bremsstrahlung from electrons interacting with surrounding medium, (2) inverse Compton emission from electrons scattering soft photons (e.g. cosmic background radiation and interstellar radiation field), and (3) proton-proton interaction producing π^0 which subsequently decay into two gamma-ray photons. In order to find an unambiguous signature of accelerated hadrons in W44, we need to clearly identify these different contributions in the high energy spectrum. As in G11, we model the gamma-ray data considering all possible emission mechanisms. We fix two important parameters obtained from radio and mm-CO data. Multifrequency radio data (Castelletti et al. 2007) provide the radio photon index $\alpha = 0.37$ that implies an electron index $p' = 1.74$, for energies less than the synchrotron peak. By using NANTEN2 telescope data, we can also fix the SNR average density in the region of gamma-ray emission at $n_{av} = 300 \text{ cm}^{-3}$.

5.1.1. Leptonic-only model failure

Our aim is to test whether a leptonic-only model can explain the gamma-ray emission from W44. We assume that the same electron population produces both the radio and the gamma-ray emissions. We assume a broken power-law electron distribution with Inverse Compton and Bremsstrahlung components.

- L1 model - We use as a parameter the index $p'_1 = 1.74$, obtained from radio synchrotron data (Castelletti et al. 2007). Relativistic bremsstrahlung has the same electron index (Blumenthal & Gould 1970). Consequently, an index $p'_1 = 1.74$ cannot explain the low-energy gamma-ray data in any way (Fig. 5, black curve). Moreover, the relation between density and magnetic field (see Appendix C) constrains the synchrotron peak; fixing the medium density to the average value found in Yoshiike et al. (2013), $n = 300 \text{ cm}^{-3}$, we cannot fit in a good way the W44 radio emission for any magnetic field value. The best model gives a $B = 25 \mu\text{G}$. Changing the density value does not improve the fit.

- L2 model - In this case, we do not apply the radio constraint on the electron spectral index in order to fit the low-energy gamma-ray data. We find that only an index $p'_1 = -2.5 \pm 0.1$ can explain the gamma-ray spectrum decay at $E < E_{br}^e$ with $E_{br}^e = 500 \text{ MeV}$, together an index $p'_2 = 3.4 \pm 0.1$ for $E > E_{br}^e$. In this case, the W44 gamma-ray emission can be explained but the radio synchrotron data (see Fig. 5, green curve) are in contradiction with the model.

Table 2. Leptonic model parameters: p'_1 is the electron spectral index before the break, p'_2 is the electron spectral index above the break, E_{br}^e is the electron break energy, and K_e is the electron normalization constant

Models	p'_1	p'_2	E_{br}^e [GeV]	K_e [1/MeV/cm ⁻³]
L1	1.74	4.2 ± 0.1	8 ± 1	4×10^{-14}
L2	-2.5 ± 0.1	3.4 ± 0.1	0.5 ± 0.1	1×10^{-11}

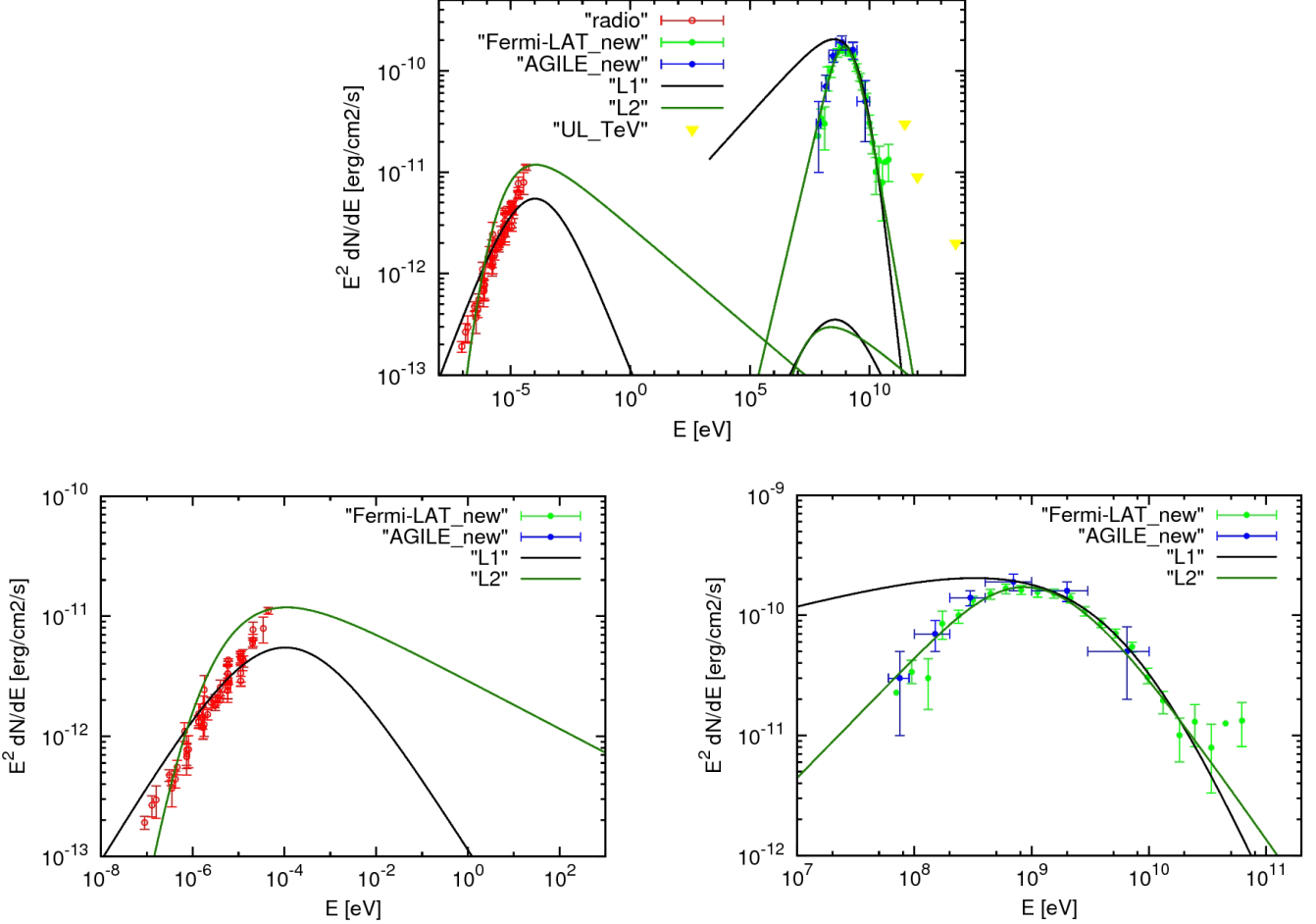


Fig. 5. Photon spectra obtained from the two leptonic-only models, L1 (green) and L2 (black), based on a broken power-law electron distribution. The density is fixed at $n = 300 \text{ cm}^{-3}$. In the model L1 the electron index is fixed at $p'_1 = 1.74$, obtained from radio data, and it provided $p'_2 = 4.2$, $B = 25 \mu\text{G}$ and $E_{br}^e = 8 \text{ GeV}$. In the model L2, instead, we obtained $p'_1 = -2.5$, $p'_2 = 3.4$, $B = 40 \mu\text{G}$ and $E_{br}^e = 500 \text{ MeV}$.

Fig. 5 shows the failure of these two models⁵, L1 and L2, to simultaneously explain the radio and gamma-ray emission of W44.

5.1.2. The best hadronic model: a broken power-law distribution

We considered different possible hadronic models (Table 1 and Fig. 3). The best one is the so called H3, a broken power-law proton distribution discussed in the following. Features and implications of the other models, H1 and H2, are discussed in Appendix A. In order to consider separately the low and high energy parts of the spectrum, we consider a non-smoothed broken power-law distribution (Eq. 3). In this way we can study which kind of processes affect one or the other part of the spectrum. We obtain a good model with $p_1 = 2.2 \pm 0.1$ for $E < E_{br}$ and $p_2 = 3.2 \pm 0.1$ for $E > E_{br}$, where $E_{br} = 20 \text{ GeV}$. The magnetic field is of the same order as for other hadronic models, $B = 210 \mu\text{G}$, and

⁵ A substantial inverse Compton contribution can be easily excluded. If the soft photon source is the Cosmic Background Radiation (CBR), we expect a second peak in the gamma-ray spectrum ($E_{peak} \sim 1 \text{ TeV}$), contradicting upper-limits from Cherenkov telescopes (Abdo et al. 2010e). If soft photons come from the InterStellar Radiation Field (ISRF), we cannot fit synchrotron radio data in any way, using reasonable magnetic field values.

the electron/proton number ratio is $\mathfrak{R} = 0.01$ at $e \sim 10$ GeV. The index found for the low-energy part is in agreement with the one found by A13. On the other hand, the high energy index of the H3 model is substantially harder than in A13 and steeper than the one found in our previous paper, $p_2 = 3.0 \pm 0.1$ (Giuliani et al. 2011). Our analysis confirms that the SNR W44 has a gamma-ray spectral index near 10 GeV steeper than all other middle-aged SNRs. Interestingly, the low-energy index near 2.3 is close to the value found in several other young SNRs (Abdo et al. 2010a; Acciari et al. 2010, 2011; Aharonian et al. 2001; Giordano et al. 2012; Hewitt et al. 2012). This fact can have a profound reason, and it may be related with a universal or quasi-universal injection of energetic particles by a SNR shock.

5.2. Hadronic models: proton energies and magnetic fields.

An important physical consequence of hadronic models is the value of the total energy going into accelerated protons. Considering the total particle energy, Castelletti et al. (2007) provided a minimum value for the total CR energy and for the magnetic field in W44, estimated from the radio data, assuming particle and magnetic energy equipartition; $U_{min} = 5.8 \times 10^{49}$ erg and $B_{min} = 13 \mu\text{G}$. For the equipartition assumption, $U_{min} = 2U_B = 2U_{CR}$. Consequently, far away from equipartition, magnetic energy should be greater than particle energy or viceversa (Longair 2011). We can use the equipartition values for magnetic and particle energies found by Castelletti et al. (2007), to expose a contradiction in their relation. Our models, except for the simple power-law with a high energy cut-off, provide a total energy in accelerated protons lower than the one calculated with the equipartition assumption, implying magnetic fields with higher values. It is essential to obtain a good estimate of the magnetic field in regions of interest in W44. In our models, in order to fit the gamma-ray data, we explicitly consider also the bremsstrahlung contribution by electrons. This approach provides a constraint on the magnetic field. Assuming that synchrotron and bremsstrahlung emissions are originated by the same electron population, both processes depend on the electron density; the higher its value, the higher their emissivity. Consequently, in order to obtain a small bremsstrahlung contribution to the gamma-ray emission with a fixed target density, the magnetic field has to be enhanced in order to obtain the correct synchrotron emission, and viceversa. The final result is that, regardless of the hadronic model, we can fit the radio data only considering a magnetic field $B \sim 10^2 \mu\text{G} \gg B_{min}$ (see Table 3). This fact implies that the magnetic energy should be the main contribution to the total energy. Consequently, our model H1 can be excluded because both magnetic and particle energies are greater than the equipartition values. Large values of the magnetic field ($B \sim 0.2$ mG) in W44 were deduced by Claussen et al. (1997) in regions near the detected OH masers. Interestingly, from Fig. 2, we find that the gamma-ray emission detected by AGILE overlaps with one of the OH maser regions. In order to obtain a large local magnetic field (i.e., substantially larger than the equipartition one) an efficient amplification mechanism must be operating. A possible mechanism was discussed by Schure et al. (2012): a linear magnetic instability can provide the condition $\delta\mathbf{B} \sim \mathbf{B}_0$. However, it is required that the instability continues to grow in order to explain magnetic fields greater than $100 \mu\text{G}$. Identifying the physical mechanisms for magnetic field amplification can be challenging. It is also important to explain the relation between magnetic field and density structures (e.g., Fig. 2 in Schure et al. 2012). In young SNRs where the ISM density is low ($n \sim 1 \text{ cm}^{-3}$), high magnetic fields are usually correlated

with optical and radio filaments. In middle-aged SNRs such as W44 surrounded by high ISM densities ($n \sim 10^2 \text{ cm}^{-3}$), the magnetic field is relatively large on wider scales.

5.3. Spectral index

Our best hadronic model is obtained from a non-smoothed broken power-law distribution. At low-energies, we can fit the gamma-ray data with a proton distribution index $p_1 = 2.2$. This value apparently agrees with the behavior seen in younger SNRs. The difference is that in young SNRs this spectral index applies also at higher energies not being affected by propagation and damping mechanisms. On the contrary, in the middle-aged SNR W44, at higher energies we find a proton index $p_2 = 3.2$, that is substantially steeper than the value expected from theoretical models without damping. Malkov et al. (2011) explained the W44 steep spectral index with the mechanism of Alfvén damping, providing a steepening of exactly one unit. However, Alfvén damping, if it occurs in W44, cannot be acting all across the proton spectrum because the deduced low-energy index seems unaffected by it.

It is interesting to compare W44 gamma-ray spectrum with the CR particle interstellar spectrum. The interstellar cosmic-ray proton spectrum results to be, in the momentum space, $p_{1,IS} = 2.5$ below $E = 6.5$ GeV and $p_{2,IS} = 2.8$ above $E = 6.5$ GeV (Dermer et al. 2013); the interstellar cosmic-ray electron spectrum, instead, seems to have an index $p'_{1,IS} = 1.3$ -1.6 below a few GeV and $p'_{2,IS} = 2.1$ -2.3 above GeV energies (Strong et al. 2011, and therein). Considering our best hadronic model, H3, it provides a proton index at the lowest energies, $p_1 = 2.2$, in the energy space. This implies a proton index in the momentum space similar to the interstellar CR spectrum one, $p_{1,m} = 2.4 - 2.5$, and the high energy proton spectral index, $p_2 = 3.2$, results to be steeper than the interstellar CR spectrum one. For the electrons, instead, radio data provided an index $p' = 1.74$ (Castelletti et al. 2007), steeper than $p'_{1,IS}$ but harder than $p'_{2,IS}$. Consequently, the CR spectral behavior in SNR W44 is different from the one of the interstellar CR spectrum. This challenging issue requires a deeper analysis beyond the scope of this paper. We note, however, that also in the interstellar case proton and electron spectra have different indices as well as in W44.

Our spectral indices are compatible with the values found in Ackermann et al. (2013), $p_1 = 2.36 \pm 0.05$ for $p < p_{br} = 22 \text{ GeVc}^{-1}$, and $p_2 = 3.5 \pm 0.3$ for $p > p_{br}$, where a smoothed broken power-law is used and there is any consideration about the electron contributions. Fang et al. (2013), instead, assumes that the W44 spectral behavior is explained by diffusive shock acceleration with ion-neutral damping and consider a lower distance of the remnant ($d \sim 1.9$) and a lower density ($n \sim 10^2 \text{ cm}^{-3}$). In this way they found a very low magnetic field ($B \sim 10 \mu\text{G}$) and a very steep spectral index, $p_1 \sim 4.1$. A direct comparison with our results is not so trivial because of the different approaches: we, as like as Ackermann et al. (2013), begin from fitting our data and then we look for a physical explanation. Fang et al. (2013), instead, begins from the issue that a linear DSA theory can explain Fermi-LAT data and then obtain the parameters that are inconsistent with both our and Ackermann et al. (2013) values.

It is interesting to remark here that data collected from the young SNRs, Tycho and Cas A (Abdo et al. 2010a; Giordano et al. 2012), show a spectral index in the range $p_1 \approx 2.2$ -2.4, i.e., steeper than the value $p_1 = 2$ predicted by idealized theoretical models (assumed by Malkov et al. 2011). Other non-linear

mechanisms modifying standard DSA, such as neutral leakage (Blasi et al. 2012b, and therein) or re-acceleration (Blasi & Amato 2012a, and therein), may substantially affect SNRs in the whole range of energies.

6. Conclusions

W44 is a crucial SNR providing important information on the CR origin in our Galaxy. However, several characteristics of this SNR deduced by a multifrequency approach (gamma-ray spectral indexes, large magnetic field) are challenging. As discussed in this paper, W44 is a relatively close and quite bright gamma-ray source. Therefore, an excellent characterization of its gamma-ray spectrum in the range 50-200 MeV has been possible because of the good statistics achieved by AGILE and Fermi-LAT. In this paper we re-analyzed the spectral properties and the likelihood of interpreting the decrement below 200 MeV as a “pion bump”. We performed a re-analysis of the AGILE data, together with revisiting radio and CO data of W44. We showed the unlikelihood of leptonic-only models in their most natural form: electron distributions constrained by radio data cannot fit the broad-band W44 spectrum. On the other hand, we find that both gamma-ray and radio data can be successfully modeled by different kinds of hadronic models (H1, H2, H3). Our results regarding the spectral properties of the accelerated proton/ion population by the W44 shock are in qualitative agreement with the results of (Giuliani et al. 2011). We provided in this paper a broader discussion of alternatives, and specified the role played by leptons alone and jointly with protons. In what follows, we summarize the most important physical characteristics of this source.

- **Neutral pion signature** - W44 is the first SNR clearly showing the so called “pion bump” that we expect at $E \geq 67$ MeV from π^0 -decay photons. The low-energy gamma-ray spectral index in our best model is $p_1 = 2.2 \pm 0.1$. This value is similar to those found in young SNRs, indicating that the proton injection spectrum is affected by non-standard mechanisms of acceleration.
- **High density of the surrounding environment** - We determined that the average density in the W44 shell is $n_{av} \sim 300 \text{ cm}^{-3}$, with $n \geq 10^3 \text{ cm}^{-3}$ in correspondence with CO peaks (see medium panels in Fig. 2). This feature was also found in other middle-aged SNRs, like W51c and IC443 (Koo et al. 2010; Castelletti et al. 2011) and explains the high gamma-ray flux detected from these sources. In the SNR W28, the average density is lower, $n_{av} \approx 5 \text{ cm}^{-3}$ (Gabici et al. 2009), but gamma-ray emission was detected in good correlation with the two MC complexes where $n \approx 10^3 \text{ cm}^{-3}$ (Giuliani et al. 2010).
- **High magnetic field** - In W44 our best hadronic models imply a magnetic field $B \geq 100 \mu\text{G}$, which is lower than the post-shock magnetic field estimated by Claussen et al. (1997) from Zeeman splitting in the OH masers, and substantially higher than the equipartition magnetic field (Castelletti et al. 2007). However, in most of SNRs, magnetic field estimations give values $B \sim 10 - 10^2 \mu\text{G}$ that are much higher than the average diffuse galactic value [see, for example, Morlino & Caprioli (2012) for Tycho, and Koo et al. (2010) and Tavani et al. (2010) for W51c and IC443, respectively]. This is hardly surprising since magnetic field compression due to the shock interaction with the ISM leads to its amplification. We need then to consider a non-linear scenario with a back-reaction of the accelerated particle at the shock (Bell et al.

2001). The large value for the magnetic field in W44 may be linked to the environment density value, $n_{av} \sim 300 \text{ cm}^{-3}$ given by NANTEN2. We notice that for a lower density value, we can enhance the electron density and make plausible a lower magnetic field.

- **Steepness of the high energy index** - As in Abdo et al. (2010e), G11, and A13, W44 shows for energies above 1 GeV, a spectral index $p_2 \sim 3$ that is steeper than the values found in other middle-aged SNRs. Alfvén damping in a dense environment (Malkov et al. 2011) is a mechanism for explaining this behavior, but other possibilities exist (e.g., Blasi & Amato 2012a; Blasi et al. 2012b). This is a point requiring deeper investigations in the future.

Our final conclusion is that W44 stands out as a crucial SNR whose gamma-ray emission can be firmly demonstrated to be of hadronic origin. A complete understanding of the W44 features requires modeling physical processes beyond DSA. Future investigations will have to address these issues as well as understanding W44 within the context of other SNRs.

Acknowledgements. We thank an anonymous referee for his/her comments that led to substantial improvements of our paper. We are pleased to thank F. Aharonian for extensive discussions that stimulated parts of the work presented in this paper. Research partially supported by the ASI grants n. I/042/10/0 and I/028/12/0 and Argentina ANPCyT and CONICET grants: PICT 0902/07, 0795/08, 0571/11, PIP 2166/08, 0736/12.

References

- Abdo, A. et al. 2009, *Astrophys. J.*, 706, L1-L6
 Abdo, A. et al. 2010a, *Astrophys. J.*, 710, 92-97
 Abdo, A. et al. 2010b, *Astrophys. J.*, 712, 459-468
 Abdo, A. et al. 2010c, *J.*, 722, 1303-13011
 Abdo, A. et al. 2010d, *Astrophys. J.*, 718, 348-356
 Abdo, A. A., et al. 2010e, *Science*, 327, 1103-1106
 Abdo, A. et al., 2011, *Astrophys. J.*, 734, 28-36
 Acciari, V.A. et al. 2009, *ApJ*, 698, 133-137
 Acciari, V.A. et al. 2010, *Astrophys. J.*, 714, 163-169
 Acciari, V.A. et al. 2010, *ApJ*, 730L, 720-725
 Ackermann, M. et al. 2011, *Science*, 334, 1103-1107
 Ackermann, M., et al. 2012, *Astrophys. J. S.*, 203, 4-73
 Ackermann, M., et al. 2013, *Science*, 339, 807-811 (A13)
 Aharonian, F. A. 2001, *Astron. Astrophys.*, 370, 112-120
 Aharonian, F. A. 2004, *Very High Energy Cosmic Gamma Radiation: a Crucial Window on the Extreme Universe*. World Scientific Publishing
 Aharonian, F. et al. 2007, *Astron. Astrophys.*, 464, 235-243
 Aharonian, F. et al. 2008, *Astron. Astrophys.*, 481, 401-410
 Aharonian, F. 2012, *Astroparticle Physics*, 43, 71-80
 Aleksic, J. et al. 2012, *Astron. Astrophys.*, 541, 13-23
 Bell, A.R. 1978a, *MNRAS*, 182, 147-156
 Bell, A.R. 1978b, *MNRAS*, 182, 443-455
 Bell, A.R. 1987, *MNRAS*, 225, 615-626
 Bell, A.R. 2001, *MNRAS*, 321, 433-438
 Berezhko, E.G. & Voelk, H.J. 2007, *Astrophys. Journal*, 661, L175-178
 Berezhinskii, V.S. et al. 1990, *Astrophysics of Cosmic Rays*, North-Holland (Amsterdam)
 Blasi, P., Gabici, S., Vannoni, G. 2005, *MNRAS*, 361, 907-918
 Blasi, P. and Amato, E. 2012a, *JCAP*, 01, 10-39
 Blasi, P. 2012b, *Astrophys. J.*, 755, 121-132
 Blumenthal, G.R. and Gould, R.J. 1970, *Reviews of Modern Physics*, 42
 Bulgarelli, A., et al. 2012, *Astron. Astrophys.*, 514, 79-90
 Butt, Y.M. 2009, *Nature*, 460, 701-704
 Castelletti, G., et al. 2007, *Astron. Astrophys.*, 471, 537-549
 Castelletti, G., et al. 2011, *Astron. Astrophys.*, 534, 21-34
 Chen, A. et al. 2013, *Astron. Astrophys.*, 558, 37-47
 Clark D.H. & Caswell J.L. 1976, *MNRAS*, 174, 267-305
 Claussen, M. J., Frail, D. A. & Goss, W. M. 1997, *ApJ*, 489, 143-159
 Claussen, M. J. 1999, *Astrophys. J.*, 522, 349-356
 Dermer, C. D. 1986, *Astron. Astrophys.*, 157, 223-229
 Dermer, C. D. 2012, *Physical Review Letters*, 109, 091101
 Dermer, C.D. et al. 2013, *ICRC*, arXiv1307.0497D
 Fang, J. et al. 2013, *MNRAS*, 435, 570-574
 Fermi, E. 1949, *Phys. Rev.*, 75, 1169-1174

Frail, D. A. et al. 1996, *Astrophys. J.*, 464, 165-169
 Fukui, Y. et al. 2012, *Astrophys. J.* 746, 82-99
 Gabici S. et al. 2009, *MNRAS*, 396, 1629-1639
 Gabici S. et al. 2007, *Astrophys. and Space Science*, 309, 365-371
 Giacani E.B. et al. 1997, 113, 1379-1390.
 Ginzburg, V.L. & Syrovatskii, S.I. 1964, *The Origin of Cosmic Rays*, Pergamon (Oxford)
 Giordano, F. et al. 2012, *Astrophys. J.*, 744, 2-6
 Giuliani, A., et al. 2004, *Mem. S.A.It. Suppl.*, 5, 135-138
 Giuliani, A., et al. 2006, *NIM A*, 568, 692-699
 Giuliani A., et al. 2010, *Astron. Astrophys.*, 516, 11-13
 Giuliani, A., Cardillo, M., Tavani, M., et al. 2011, *Astrophys. J.* 742, 30-34 (G11)
 Gomez, H.L. 2012, *Mon. Not. R. Astron. Soc.*, 420, 3557-3573
 Helder, E.A. et al. 2012, *Space Science Reviews*, 173, 369-431
 Hewitt, J.W. et al. 2012, *Astrophys. J.*, 759, 89-98
 Hoffman, M., Goss, W. M., Brogan, C. L. and Claussen, M. J. 2005, *Astronom. J.*, 620, 257-273
 Hunter, S. D. et al. 1997, *Astrophys. J.*, 481, 205
 Hwang, U. & Laming, J.M. 2012, *Astrophys. J.*, 746, 130-147
 Inoue, T. et al. 2012, *Astrophys. J.*, 744, 71-85
 Katsuta, J. 2012, *Astrophys. J.*, 752, 135-146.
 Kelner, S. R., Aharonian, F. A., & Bugayov, V. V. 2006, *Phys. Rev. D*, 74, 034018
 Koo, B et al. 2010, *Astronom. J.*, 140, 262-265
 Lemoine-Goumard, M. 2012, *Astron. Astrophys.*, 545, 28-36
 Longair, M. 2011. *High Energy Astrophysics*. Cambridge University Press. Third edition.
 Malkov, M.A. & Drury, O. 2001, *Rep. Prog. Phys.*, 64, 429-481
 Malkov, M.A., Diamond P.H. & Sagdeev, R.Z. 2011, *NatCo*, 2, 194-198
 Mori, M. 1997, *ApJ*, 478, 225-232
 Morlino, G. & Caprioli, D. 2012, *Astron. Astrophys.*, 538, 81-95
 Onic, D. 2013, arXiv:1304.1766
 Picozza, P. et al. 2007, *Proc. ICR*
 Reach, W.T., et al. 2005, *AJ*, 618, 297-320
 Rho, J., et al. 1994, *AJ*, 430, 757-773
 Schure, K.M. et al. 2012, *Space Science Reviews*, 173, 491-519
 Shelton, R.L., Kuntz, K.D., Petre, R. 2004, *ApJ*, 611, 906-618
 Simpson, J.A. 1983, *Ann. Rev. Nucl. Part. Sci.*, 33, 323-81
 Skilling, J. & Jones, A.W. 1976, *Astron. Astrophys.*, 53, 253-258
 Strong, A.W. et al. 2004, *A&A*, 422, 47-50
 Strong, A.W., Orlando, E. & Jaffe, T.R. 2011, *Astron. Astrophys.*, 534, 54-66
 Taylor, J.R. 2000 *An Introduction to Error Analysis: The Study of Uncertainties in Physical Measurements*. University Science Books.
 Tavani, M. et al. 2008, *A&A*, 502, 995-1013
 Tavani, M. et al. 2010, *Astrophys. J.*, 710, 151-155
 Torres D.F. et al. 2003, *Physics Reports*, 382, 303-380
 Uchiyama, Y., et al. 2012, *Astrophys. J.* 749, 35-39
 Vercellone, S., et al. 2008, *ApJ*, 676, L13-L16
 Vercellone S., et al. 2009, *ApJ*, 690, 1018-1030
 Vink, Y. 2012, *Astron. Astrophys. Rev.*, 20, 49-168
 Watson, M. G., et al. 1983, *IAUS*, 101, 273-280
 Wolszczan, A., et al. 1991, *AJ*, 372, L99-L102
 Wootten, H.A. 1977, *ApJ*, 216, 440-445
 Yoshiike, S. 2013, *Astrophys. J.*, 768, 179-188

Appendix A - Old and new AGILE and Fermi-LAT data on W44

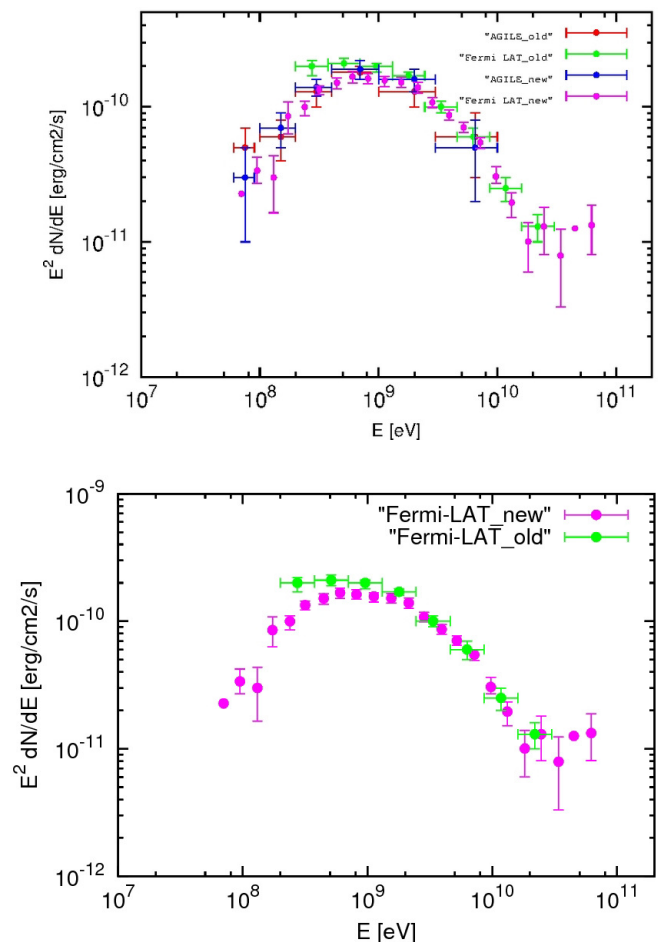


Fig. 6. (Top Panel): AGILE (red) and Fermi-LAT (green) old spectral energy distribution (SED) of W44 (Giuliani et al. 2011; Abdo et al. 2010e), together with the new Fermi-LAT (magenta) (Ackermann et al. 2013). The new AGILE data are shown in blue in Fig. 1. **(Bottom Panel):** Fermi-LAT new (magenta) (Ackermann et al. 2013) and old (green) (Abdo et al. 2010e) spectral energy distributions. We note that there is a substantial difference at low-energies between the two data set.

Fig. 6 shows the old and new AGILE and Fermi-LAT spectral energy distribution (SED) of W44. Low-energy spectral points have been added to the Fermi-LAT spectrum because to its recently improved analysis (Ackermann et al. 2012). We notice that the low-energy Fermi-LAT spectrum below 200 MeV has changed with respect to the previous Fermi-LAT data of Abdo et al. (2010e). On the other hand, the AGILE data re-analyzed in this paper are no so different from those previously presented in G11 except for the lowest energy point between 50-100 MeV. This lowest-energy spectral data is lower than the one found in our previous paper, and agrees with the Fermi-LAT spectral trend. Constraining the gamma-ray spectrum near 50 MeV is of the greatest importance for its relevance related with a possible bremsstrahlung contribution.

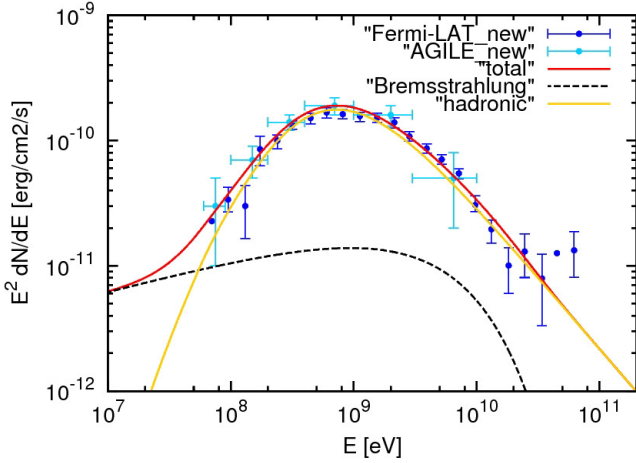


Fig. 7. Hadronic model H1 of the gamma-ray spectrum of W44 superimposed with the gamma-ray data of Fig. 1 (in blue and cyan color). We find an index $p_1 = 2.0 \pm 0.1$ with a high-energy cut-off at $E_c^p = 45$ GeV. This model is characterized by $B = 210 \mu\text{G}$ and $n = 300 \text{ cm}^{-3}$. The yellow curve shows the neutral pion emission from the accelerated proton distribution discussed in the text. The black dashed curve shows the electron contribution by bremsstrahlung (dashed) emissions. The IC contribution is negligible. The red curve shows the total gamma-ray emission from pion-decay and bremsstrahlung.

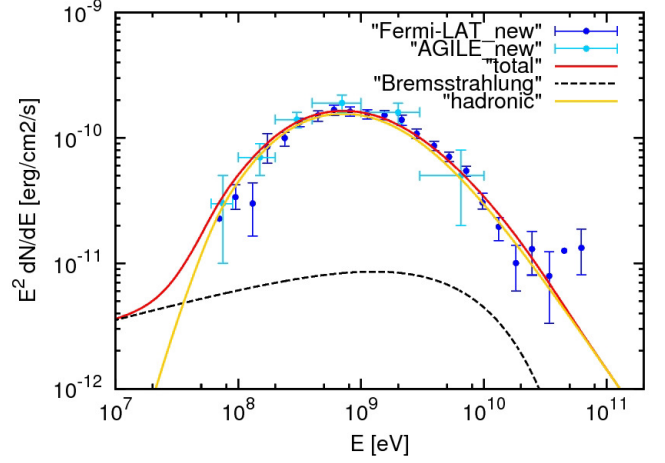


Fig. 8. Hadronic model H2 of the gamma-ray spectrum of W44 superimposed with the gamma-ray data of Fig. 1 (in blue and cyan color). We find an index $p_1 = 1.74.0 \pm 0.1$ (for $E < E_{br}$), $p_2 = 3.5 \pm 0.1$ (for $E > E_{br}$) where $E_{br}^p = 16$ GeV. This model is characterized by $B = 210 \mu\text{G}$, and $n = 300 \text{ cm}^{-3}$. The yellow curve shows the neutral pion emission from the accelerated proton distribution discussed in the text. The black dashed curve shows the electron contribution by bremsstrahlung (dashed) emissions; the IC contribution is negligible. The red curve shows the total gamma-ray emission from pion-decay and bremsstrahlung.

Appendix B - Other hadronic models

Simple power-law with a high-energy cut-off

Following Aharonian (2004), we fit our W44 spectral data with a simple power-law with a high-energy cut-off. In this case, our best-fitting parameters are an index $p_1 = 2.0 \pm 0.1$, and a cut-off energy at $E_c^p = 45$ GeV with $B = 210 \mu\text{G}$. Deduced global physical quantities are a relatively large proton energy, $W_p = 1.2 \times 10^{50}$ erg, and a low electron/proton energy ratio $\mathcal{R} = 0.005$. Even in this case, there are some points against the applicability of this model. First, we can only fit our data with this proton distribution ignoring the last four Fermi high energy points, and requiring a very low electron/proton ratio. Moreover, the high-energy cut-off considered in Aharonian (2004) for a SNR of similar age as W44 in similar density and magnetic field conditions is less sharp than the one obtained in our model, even with a high diffusion coefficient.

Smoothed broken power-law

Another way to model the W44 gamma-ray spectral data is using a smoothed broken power-law proton distribution (Eq.2). Our best model provides indices $p_1 = 1.74 \pm 0.1$ for $E < E_{br}$, and $p_2 = 3.5 \pm 0.1$ for $E > E_{br}$, with $E_{br} = 16$ GeV, $B = 210 \mu\text{G}$ and $\mathcal{R} = 0.08$. We notice that for this proton distribution, we obtain the same index of the electron distribution. In our opinion, however, the distribution of Eq.2 cannot be considered a good model. The reason is that this model introduces a strong covariance between the low- and high-energy indices making their determination quite difficult and questionable. We demonstrate this point by showing in Fig. 10 the pion emission expected from proton distribution of difference indices extending to the lowest energies and with no breaks at higher energies. The low-energy part of the spectrum of W44 can be well fitted by an index in a range 2 – 2.3. Steeper or harder indices cannot reproduce our data, this

being true also for the value $p_1 = 1.74 \pm 0.1$ found with the approach considered here.

Simple power-law with a low-energy cut-off

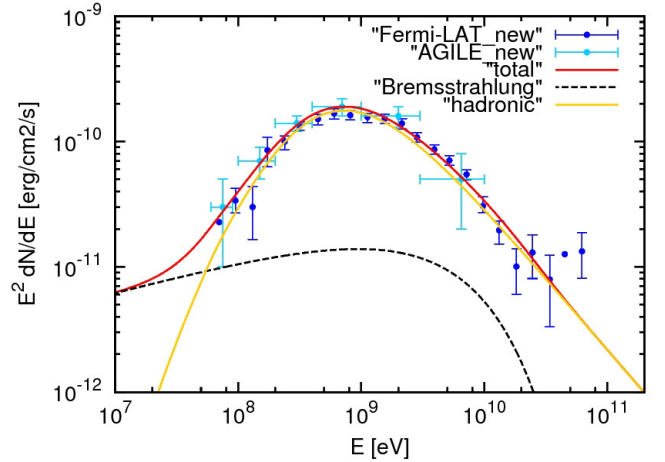


Fig. 9. Hadronic model H4 of the gamma-ray spectrum of W44 superimposed with the gamma-ray data of Fig. 1 (in blue and cyan color). We find an index $p_1 = 3.2 \pm 0.1$ with a low-energy cut-off at $E_c^p = 6.5$ GeV. This model is characterized by $B = 145 \mu\text{G}$ and $n = 300 \text{ cm}^{-3}$. The yellow curve shows the neutral pion emission from the accelerated proton distribution discussed in the text. The black dashed curve shows the electron contribution by bremsstrahlung (dashed) emissions; the IC contribution is negligible. The red curve shows the total gamma-ray emission from pion-decay and bremsstrahlung.

In our previous paper G11, we used a simple power-law proton distribution in kinetic energy which resulted in a spectral index $p_1 = 3.0 \pm 0.1$, and a low-energy cut off at $E_{k,c}^p = 5.5$ GeV.

We model here the W44 spectral data with the same kind of distribution as in G11, but in total energy rather than kinetic energy, as justified by the approach of Kelner et al. (2006):

$$\frac{dN_{p,4}}{dE} = K_p E_k^{-p} e^{-\frac{E_k^p}{E}} \quad (9)$$

We obtain a reasonable good modeling of the spectral data with an index $p_1 = 3.2 \pm 0.1$, and a cut-off energy $E_c^p = 6.5$ GeV, for a magnetic field $B = 145 \mu\text{G}$, and an electron/proton energy ratio $\mathcal{R} = W_e/W_p = 0.03$. If the interaction of protons with the gas is outside the acceleration site, the energy-depended diffusion of particles may produce this cutoff, as observed for the SNR W28 (Giuliani et al. 2010) and discussed by (Gabici et al. 2009). Alternatively, it may be due to a suppression of the diffusion coefficient due to turbulent motions in the cloud (Gabici et al. 2007) that would exclude the low-energy CRs from the denser regions. In both cases a slow diffusion coefficient ($D \sim 10^{26} \text{ cm}^2 \text{ s}^{-1}$ at 10 GeV) is required.

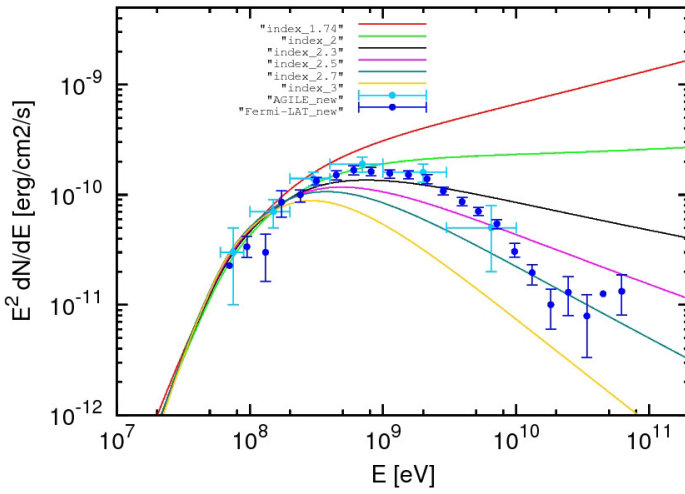


Fig. 10. Gamma-ray emission from neutral pion decay calculated for different simple power-law proton distributions of different spectral indices without any break or cut-off. We show the cases for $p_1 = 1.74$ (red), $p_1 = 2$ (green), $p_1 = 2.3$ (black), $p_1 = 2.5$ (magenta), $p_1 = 2.7$ (cyan), and $p_1 = 3$ (yellow).

Appendix C - Density and magnetic field link

The relation between the magnetic field and the target density in W44 is important for our modeling. We consider here a hadronic model with the same parameters of our best model (broken power-law distribution, see Table 3) but with higher density values, $n = 1000 \text{ cm}^{-3}$ and $n = 2000 \text{ cm}^{-3}$. We assume that all gamma-ray emission detected by AGILE originates from the core of the W44 molecular cloud at Galactic coordinates (34.75,-0.5). In Fig. 11 (top panel), we show the results obtained with these high density values together with the one obtained for $n = 300 \text{ cm}^{-3}$. The higher the density, the higher the bremsstrahlung contribution to the total gamma-ray emission. A too large value of the target density may lead to an over-estimation of the high energy gamma-ray data. The only way to fit the data is by assuming a lower electron density (and a lower electron/proton energy ratio $\mathcal{R} = W_e/W_p$) with a consequently higher magnetic field, $B \sim 410 \mu\text{G}$ and $B \sim 1110 \mu\text{G}$ for $n = 1000 \text{ cm}^{-3}$ and $n = 2000 \text{ cm}^{-3}$, respectively (Fig. 11, bottom panel).

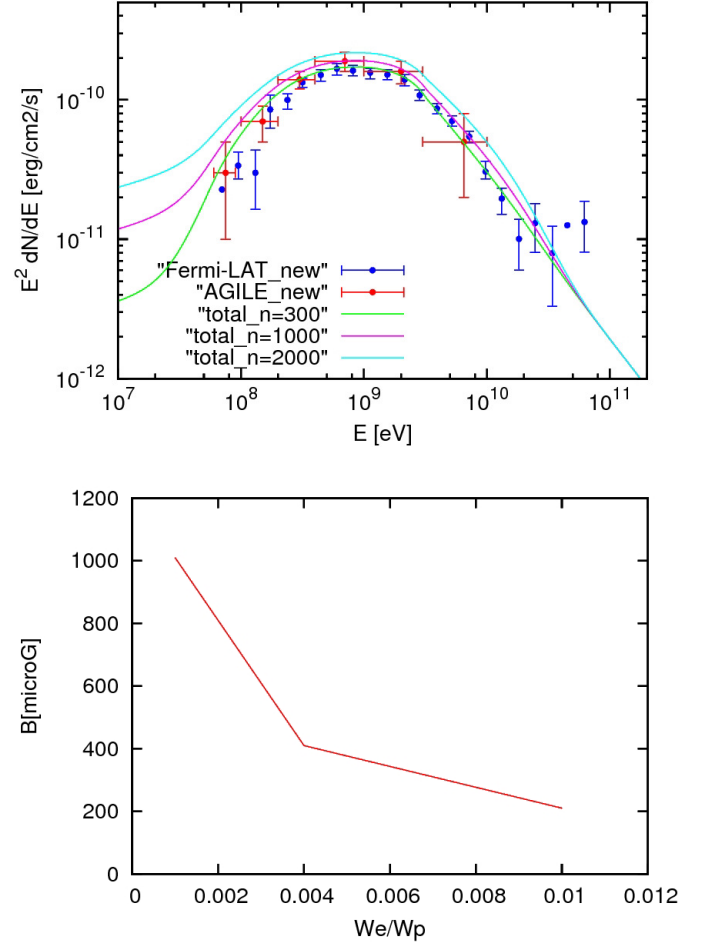


Fig. 11. (Top Panel): Our best hadronic model H3 (see Fig. 4), for three different values of the target density; $n=300, 1000, 2000 \text{ cm}^{-3}$. **(Bottom Panel):** correlation between the magnetic field and the electron/proton ratio in order to fit the spectral gamma-ray data of W44 for the three assumed target densities.

Table 3. Summary of the model parameters used in order to fit gamma-ray and radio W44 data. $\langle B \rangle$ is the average magnetic field, $\langle n \rangle$ is the average density, E_{br}^p and E_{br}^e are the proton and electron break energies, E_c^p and E_c^e are the proton and electron cut-off energies, p_1 and p_2 are the proton indices below and above the break, p'_1 and p'_2 are the electron indices below and above the break, W_p and W_e are the proton and electron total energies.

Models	$\langle B \rangle$ [μG]	$\langle n \rangle$ [cm^{-3}]	E_{br}^p [GeV]	E_c^p [GeV]	E_{br}^e [GeV]	E_c^e [GeV]	p_1	p_2	p'_1	p'_2	W_p [erg]	W_e [erg]
Giuliani et al. (2011)	70	100	-	5.5 ± 1 (LE)	-	15 ± 1	3.0 ± 0.1	-	1.74	-	3.3×10^{49}	2.8×10^{48}
Ackermann et al. (2013)	-	100	22 ± 1	-	-	-	2.36 ± 0.05	3.5 ± 0.3	-	-	4×10^{49}	-
H1	210	300	-	45 ± 1 (HE)	-	20 ± 1	2.0 ± 0.1	-	1.74	-	1.2×10^{50}	6.4×10^{47}
H2	210	300	16 ± 1	-	-	15 ± 1	1.7 ± 0.1	3.5 ± 0.1	1.74	-	1.3×10^{49}	9.6×10^{48}
H3	210	300	20\pm1	-	-	12\pm1	2.2\pm0.1	3.2\pm0.1	1.74	-	5×10^{49}	5.6×10^{47}
L1	25	300	-	-	8 ± 1	-	-	-	1.74	4.2 ± 0.1	-	3.2×10^{48}
L2	40	300	-	-	0.5 ± 0.1	-	-	-	-2.5 ± 0.1	3.4 ± 0.1	-	6.6×10^{47}